Available online at www.sciencedirect.com
ScienceDirect
Tetrahedron
Tetrahedron 63 (2007) 7349–7357

Self-assembled hybrid nanofibers confer a magnetorheological supramolecular hydrogel☆

Zhimou Yang,[a] Hongwei Gu,[a] Jun Du,[b] Jinhao Gao,[a] Bei Zhang,[b] Xixiang Zhang[b] and Bing Xu[a,*]

[a]*Department of Chemistry, The Hong Kong University of Science and Technology, Clear Water Bay, Hong Kong, China*
[b]*Department of Physics, The Hong Kong University of Science and Technology, Clear Water Bay, Hong Kong, China*

Received 2 November 2006; revised 23 January 2007; accepted 1 February 2007
Available online 7 February 2007

Abstract—Most magnetorheological materials, composed of magnetic microparticles in a liquid, require significant amounts of magnetic particles and a large magnetic field to achieve the desired effects. Here, we report on a new type of magnetorheological materials consisting of small amounts of magnetic nanoparticles (0.8 wt %) but exhibiting large rheological change (i.e., a gel–sol transition) upon the application of a small magnetic field. We use self-assembly to create hybrid nanofibers, which consist of supramolecular hydrogelators and magnetic nanoparticles, as the matrices of the hydrogel. Localized in the nanofibers at a distance of 1–2 nm, the magnetic nanoparticles occupy a small volume fraction of the hydrogel, significantly enhancing the magnetic dipole interactions between them, which results in the large magnetoresponse. This strategy generates a hierarchical nanostructure and eliminates several drawbacks of the simple mixture of polymers with nanoparticles, and thus provides a new methodology that uses magnetic force to control the nanostructures and properties of soft materials.

1. Introduction

Conventionally, magnetorheological (MR) materials are MR fluids and ferrofluids that exhibit responses to a magnetic field but are distinct from each other.[1,2] In an MR fluid, magnetic microparticles (typical diameters in the order of 1–10 μm) are suspended in a liquid (e.g., silicon oil) under zero field; the microparticles form fibrous aggregates aligned with an applied magnetic field to display a dramatic change in rheological properties. In a ferrofluid, magnetic nanoparticles (with diameters in the order of 1–10 nm) are dispersed in a liquid; the ferrofluid shows a relatively small change in viscosity upon the application of a magnetic field because the Brownian motion of the nanoparticles disfavors the formation of stable fibrous aggregates. Though they seem unrelated, supramolecular hydrogels share some common features with the MR fluids. In a supramolecular hydrogel,[3–8] the self-assembly of small molecules (i.e., the hydrogelators) forms nanofibers with an external stimulus, temperature, pH, ionic strength, or mechanical agitation[3,4] to dramatically change the viscoelastic behavior of the materials (e.g., sol–gel or gel–sol phase transitions). Comparable in size to hydrogelators, magnetic nanoparticles[9–12] may cooperatively interact with the nanofibers formed by the hydrogelators. If a magnetic field causes formation or dissociation of the hybrid nanofibers of magnetic nanoparticles and hydrogelators, a large rheological change should take place and result in an MR material. Although no report has described such an MR supramolecular hydrogel, several reports demonstrated magnetoresponses in polymeric gels that contain magnetic nanoparticles (e.g., ferrogels[13]). Although the responses are relatively weak (i.e., the gel only changes its shape) in those systems, these works,[13–17] nevertheless, confirm that it is possible to magnetically influence the rheological properties of molecular aggregates in a gel by introducing magnetic nanoparticles into the gel.

In a polymeric gel mixed with magnetic nanoparticles, the magnetic nanoparticles upon the application of a magnetic field are unable to break up the polymer network (even when the nanoparticles are covalently attached to the polymer chains as pendants). Therefore, an insufficient interaction between the magnetic nanoparticles and the polymeric matrices of the gels limits the magnetic response and fails to cause a large rheological change. On the other hand, rational design of an amphiphilic molecule allows the control of hydrogen bonding and hydrophobic interactions among the molecules themselves and between the molecules and a solvent, thus leading to self-assembled nanofibers (i.e., a type of supramolecular architecture) of the amphiphilic molecules in the solvent, which yield an organogel[3] or a hydrogel.[4] Unlike conventional polymer networks, such nanofibers form reversibly, providing an opportunity to incorporate magnetic nanoparticles into them. Following this notion, we created a new type of supramolecular hydrogel, in which the matrices are made of self-assembled nanofibers of small molecules

☆ This work was partially supported by RGC (Hong Kong), EHIA (HKUST).
* Corresponding author. E-mail: chbingxu@ust.hk

0040–4020/$ - see front matter © 2007 Elsevier Ltd. All rights reserved.
doi:10.1016/j.tet.2007.02.009

and surface-modified magnetic nanoparticles to induce phase transitions of the hydrogel by a magnetic force. As shown in Scheme 1, this new architecture relies on the molecular interactions between the hydrogelators and the magnetic nanoparticles to form hybrid nanofibers for hydrogelation. Subjected to a non-uniform magnetic field, the well-distributed magnetic nanoparticles in the nanofibers respond to the magnetic field to disrupt the hybrid supramolecular network to lead to a gel–sol transition.

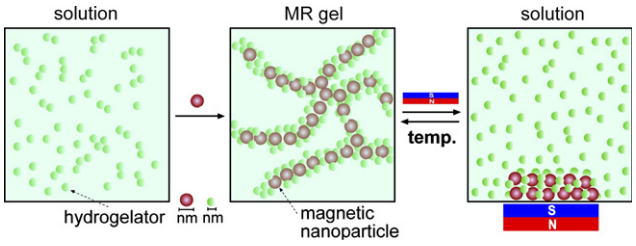

Scheme 1. An illustration of a magnetorheological supramolecular hydrogel based on hybrid nanofibers consisting of hydrogelators and magnetic nanoparticles.

2. Results and discussions

To create the system depicted in Scheme 1, we synthesized a small molecule hydrogelator (**1**) and examined its ability to form a hydrogel. Compound **1** is a dipeptide derivative, made by conjugating 2-(naphthalen-2-yl) acetic acid with Phe–Phe, a diamino acid residue that has been shown to self-assemble.[18] In the molecule of **1**, the napthanyl group ($C_{10}H_7CH_2$–) provides the hydrophobic force to enhance self-assembly in the aqueous environment; the amide groups on the dipeptide segment (Phe–Phe) act as both the acceptors and the donor of hydrogen bonds. We find that **1** is an effective hydrogelator that forms a hydrogel at a concentration of 0.8 wt %, with the gel–sol transition temperature at about 323 K. A transmission electron micrograph (TEM) reveals that **1** self-assembles to create nanofibers with widths of 18–45 nm and lengths longer than microns (Fig. 1a). These

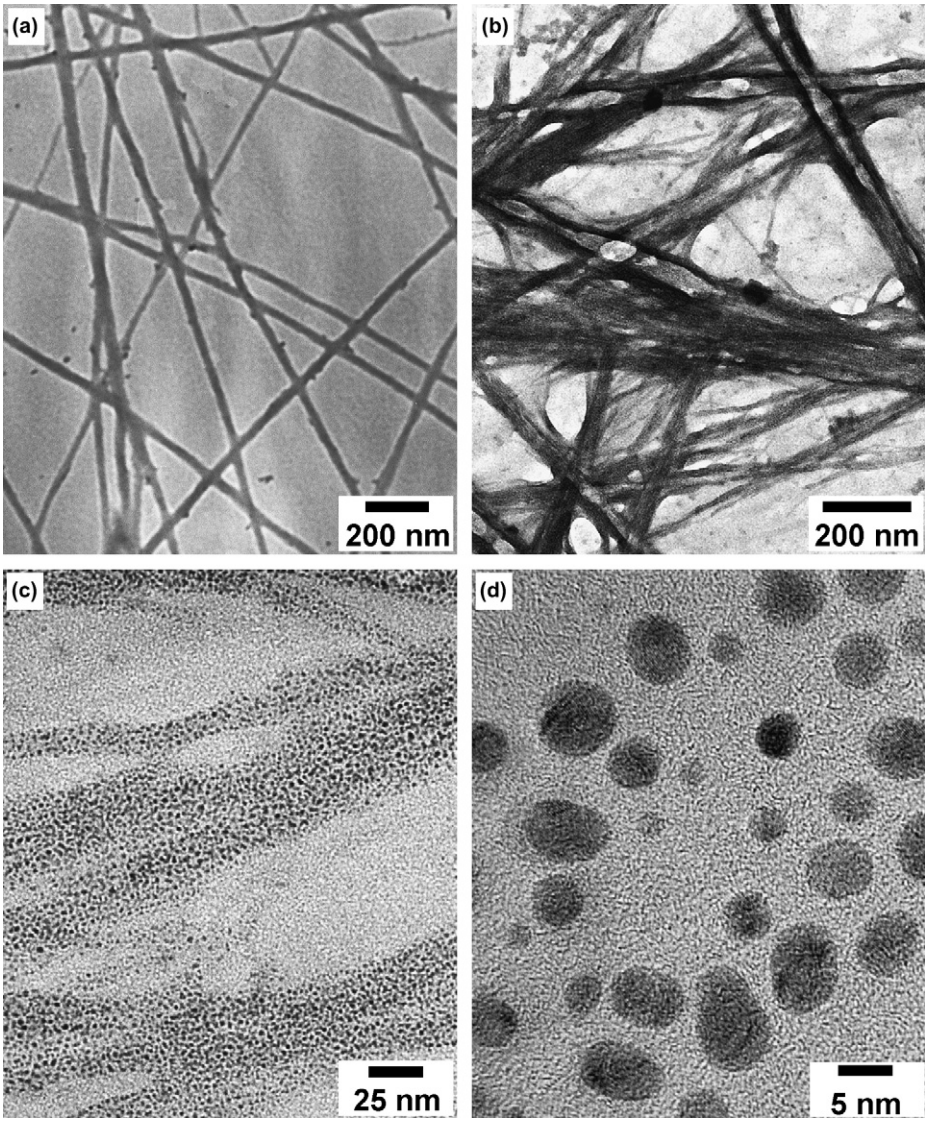

Figure 1. Cryo-TEM images of (a) the hydrogel of **1**; (b) the hydrogel formed by adding magnetite nanoparticles (0.8 wt %) into the solution of **1** (0.35 wt %); (c, d) higher magnification of (b).

fibers constitute the matrices (in the form of bundles or networks) of the hydrogel.

After proving the effectiveness of **1** in forming a hydrogel, we added dopamine–modified Fe_3O_4 nanoparticles (DA–Fe_3O_4) into the hydrogel (1.0 wt % of the hydrogelator). Neither a phase transition nor a significant shape change of the hydrogel was observed over 24 h with the application of a small magnetic force to the mixture. TEM analysis of the mixture reveals that the nanofibers of **1** are unable to incorporate the DA–Fe_3O_4 nanoparticles (Fig. 2). To ensure an adequate interaction between the nanoparticles and the nanofibers of **1**, we synthesized **2** (using dopamine as the anchor) to modify the surface of Fe_3O_4 (Schemes 2 and 3).[19] The addition of the **2**–Fe_3O_4 conjugate (0.8 wt %) into the solution of **1** (0.35 wt %) converts the solution (Fig. 3a) into a transparent hydrogel ($T_{gel-sol}$ is about 325 K, Fig. 3b). Upon the application of a small bar magnet (0.33–0.11 T, the field is 0.33 T near the surface of the magnet), the hydrogel responds to the magnetic force and turns into a solution with the nanoparticle precipitate attracted by the magnet (Fig. 3c,d). A simple heating/cooling procedure regenerates the hydrogel. This cycle can be repeated many times.

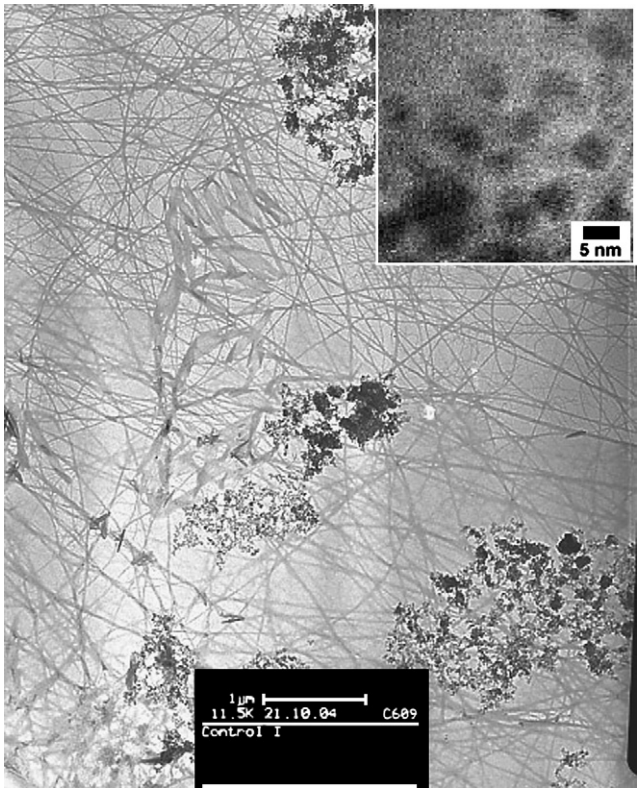

Figure 2. TEM image of the hydrogels formed by 1.0 wt % of Nap–FF and 0.8 wt % of DA–Fe_3O_4 (the aggregation of the nanoparticles is caused by cryo-drying).

TEM analysis of the hydrogel in Figure 3b shows that the nanofibers are from 20 to 30 nm in size (Fig. 1b) and the nanoparticles of **2**–Fe_3O_4, one of the structural components, are distributed rather evenly in the nanofibers (Fig. 1c,d), which fits the model depicted in Scheme 1. This morphology also explains the gel–sol transition upon the application of a small magnet. When a non-uniform magnetic field (e.g., as from a small bar magnet) is applied to the hydrogel, the movement of the magnetic nanoparticles toward the magnet causes the hybrid nanofibers to collapse. Because the remaining molecules of **1** fail to reach a high enough density to form the nanofiber matrices for gelation, the hydrogel becomes a solution, as shown in Figure 3d and illustrated in Scheme 1.

To help elucidate the molecular details in this system, we obtained the crystal structure of **1** (CCDC 632302: www.ccdc.cam.ac.uk/data_request/cif) from ethanol because the arrangement of the molecules in the nanofibers may adopt similar molecular packing in its solid state. As shown in Figure 4a, one molecule of **1** forms six hydrogen bonds with four other surrounding molecules of **1**, two from above and two from below. This supramolecular arrangement not

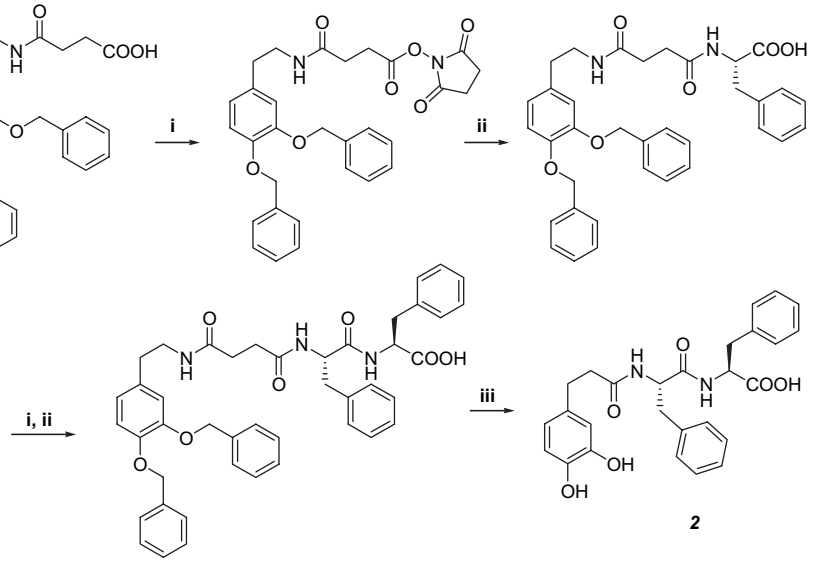

Scheme 2. Chemical structure and synthetic scheme of compound **2**. (i) DCC, NHS, dimethoxy ethane; (ii) L-phenylalanine, $NaHCO_3$, H_2O/acetone; (iii) Pd/C, methanol.

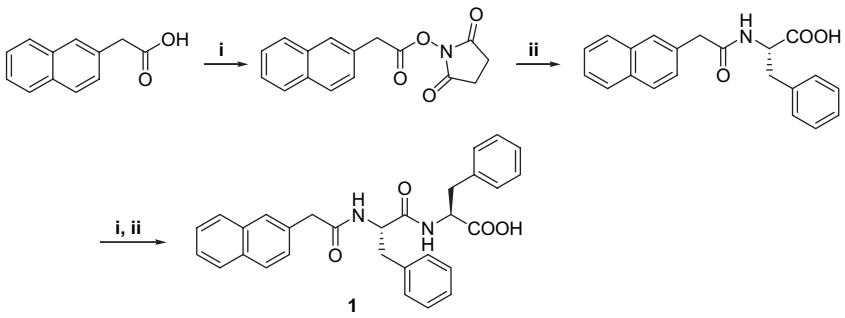

Scheme 3. Chemical structure and synthetic scheme of compound **1**. (i) DCC, NHS, dimethoxy ethane; (ii) L-phenylalanine, $NaHCO_3$, H_2O/acetone.

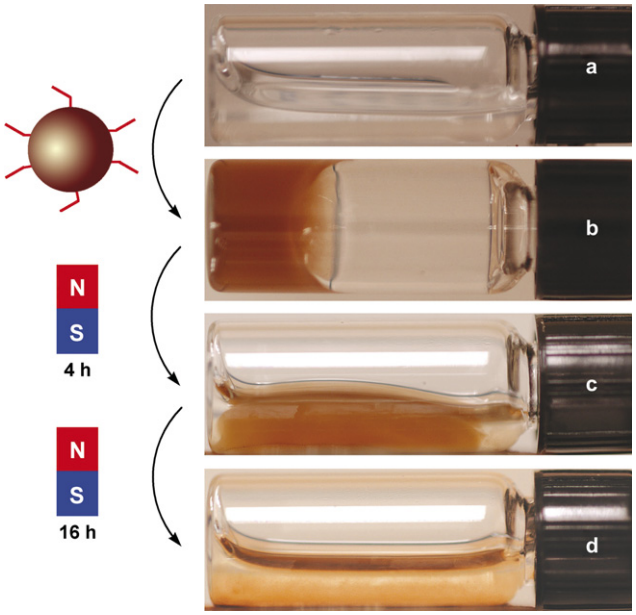

Figure 3. Gelation by adding magnetite nanoparticles and a magnet-induced gel–sol transition. (a) Solution of **1** (0.35 wt %); (b) the hydrogel contain **1** and **2**–Fe_3O_4; (c) the shape change of the hydrogel after application of the magnet; (d) the solution of **1** and the precipitate of **2**–Fe_3O_4.

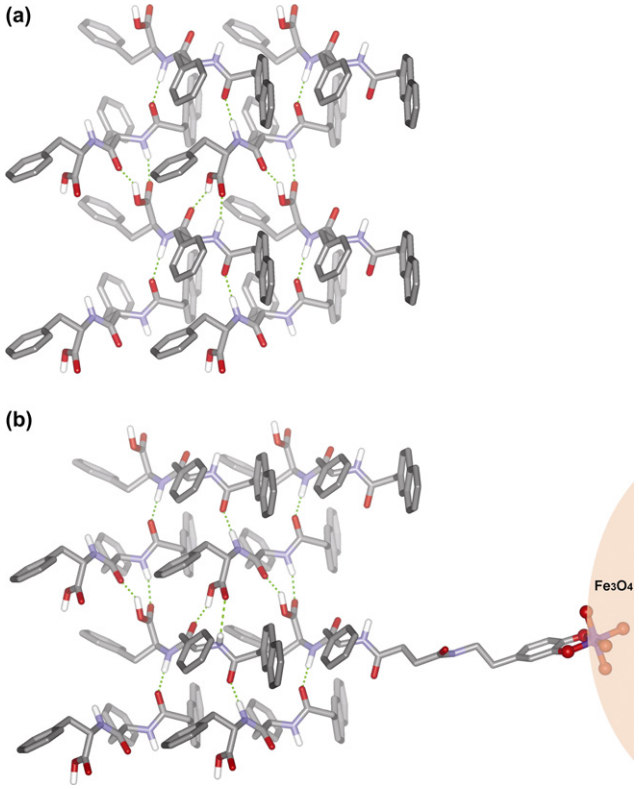

Figure 4. Molecular packing of the hydrogelator **1** (a) in the crystal phase and (b) interacting with the surface bound molecules of **2** in a plausible model based on (a).

only permits a chain-like structure, but also allows the surface-bounded molecule of **2** on a nanoparticle to insert into the chain of **1** (Fig. 4b). With the extension of such structures, the hybrid nanofibers containing the conjugate of **2**–Fe_3O_4 are generated, as shown in Figure 5. These hybrid nanofibers form a hierarchical nanostructure: the self-assembly of **1** affords the primary structure—supramolecular chains; the non-covalent interactions allow the incorporation of **2**–Fe_3O_4 into the chains to give the secondary structure—hybrid nanofibers. This hierarchical arrangement localizes the magnetic nanoparticles in a small volume fraction, which results in the observed large magnetoresponse (vide infra).

To understand the interactions between the magnetite nanoparticles within the hybrid nanofibers, we characterized the magnetic properties of the supramolecular hydrogels containing hybrid nanofibers (the 'sample') and its corresponding control (i.e., DA–Fe_3O_4 mixed in the hydrogel of **1**, the 'control'). The zero-field-cooling and field-cooling (ZFC–FC) magnetization curves (with a field of 50 Oe and from 5 to 360 K, Fig. 6a) of the control display a broad peak at ~54 K in the ZFC curve, corresponding to the unblocking of the magnetic moment of the DA–Fe_3O_4 nanoparticles.[20] Since magnetic nanoparticles generally exhibit uniaxial anisotropy, by using T_B~54 K and the magnetic anisotropy constant, $K=1.1\times10^4$ J/m^3 for Fe_3O_4,[21] we can estimate the diameters of the nanoparticles to be 7.3 nm (based on the relation of $KV=25K_BT_B$[20]). This value matches with the average diameter obtained from the TEM image (7.5 nm from Fig. 1d). Above the T_B, the magnetization data follow the Curie law, $M\sim1/T$, as seen in Figure 6b, indicating very weak magnetic dipole–dipole interactions between the nanoparticles. The peak at around 287 K in the ZFC curve is due to the transition from the solid to the hydrogel, at which point the particles rotate physically (in addition to the rotation of the magnetic moments of the nanoparticles) due to the elasticity of the hydrogel. After the onset of the

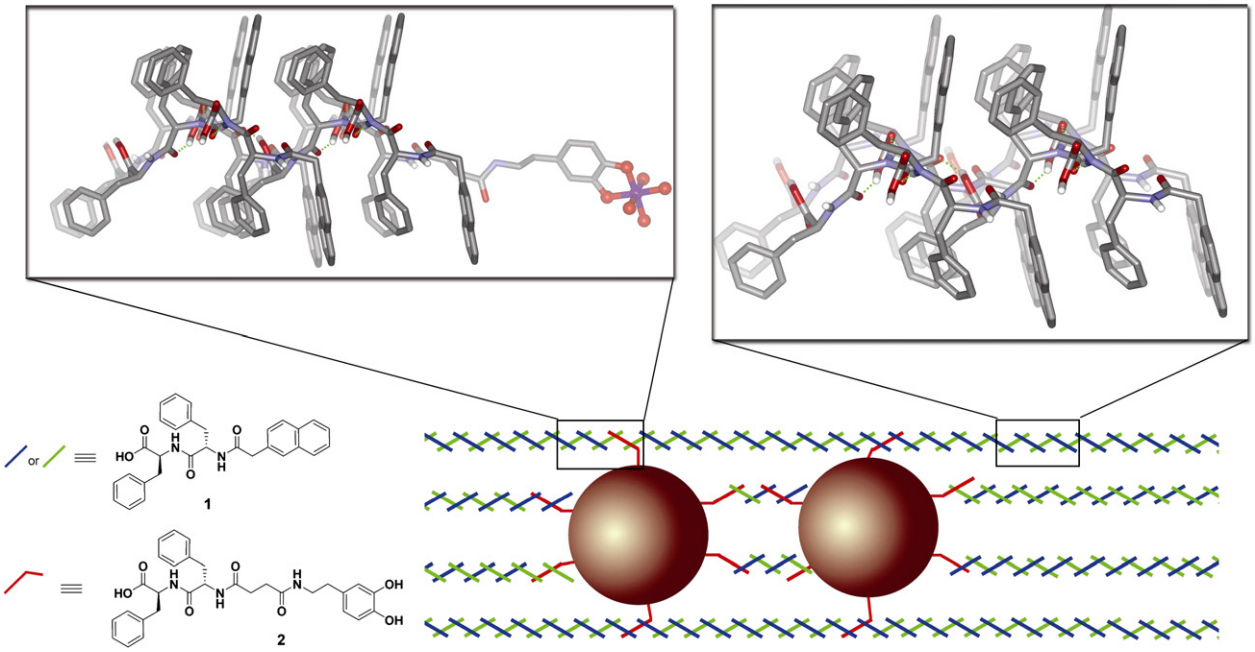

Figure 5. Plausible supramolecular interactions in the hybrid nanofibers.

physical rotation of the particles, the easy axes of the particles further align with the field direction, which explains the sharp, up-displacement of the curves above the solid-to-gel transition. The dip at 320 K originates from the gel–sol phase transition. Near this transition, the system might undergo a drastic change due to the release of stress caused by the magnetic torque (although the elastic constant of the gel is not large). In this process, the misaligned easy axes of the nanoparticles cause a drop in the magnetic moment. Once the gel–sol transition is complete, the magnetic field realigns the easy axes. Because the nanoparticles are more physically free in the liquid phase than in the gel phase, the magnetic moment of the sample not only recovers its value, but also shows a small up-displacement. The overall FC curve is typical for a non-interacting nanoparticle system. The small, sharp dip at around 250 K is due to the freezing of the liquid when the sample is cooled. At this point, the sample undergoes a dramatic phase transition, and the physical motion of the particles is suddenly ruled out. During this transition, the alignment of easy axes becomes frustrated, which cause a sharp dip in the magnetization. Another reason might be that the latent heat of the first-order phase transition is absorbed by the magnetic nanoparticles, which leads to a rise in the actual temperature of the nanoparticles. This increase in the temperature of the nanoparticles would cause a decrease in the magnetization because the magnetization follows the Curie law. The alternating current (ac) susceptibility data obtained from the control are shown in Figure 6c. Analysis of the susceptibility data reveals that the nanoparticles do not interact. The high temperature data (measured from 290 to 350 K) show the superparamagnetic behavior of the nanoparticles and the completion of the gel–sol phase transition at 327 K.

As indicated by TEM (Fig. 1), the **2**–Fe_3O_4 nanoparticles are incorporated in the hybrid nanofibers by supramolecular interactions (i.e., π–π interactions and hydrogen bondings), which bring the nanoparticles together at a distance as small as 1–2 nm. In this case, the magnetic dipole–dipole interaction between the nanoparticles should be significant. Therefore, one expects very different behavior from the **2**–Fe_3O_4 nanoparticles in the sample.

As shown in Figure 6d, the ZFC–FC curves of the sample are indeed distinct from those of the control, showing a peak at about 16 K and an additional broad peak at about 245 K. It is well known that a peak in a ZFC curve of a magnetic nanoparticle system is due to unblocking of the magnetic moment (moment flipping by overcoming the anisotropy energy due to the thermal agitation). The position and the broadness of the peak should be determined by the size distribution of nanoparticles and the direction of the easy axes.[22] Therefore, the peak at 16 K is due to the unblocking of the isolated (or non-coupled) magnetic nanoparticles. From the peak temperature (T_B=16 K), we can estimate that the average diameter of these particles is about 5 nm, coinciding with the sizes of **2**–Fe_3O_4 nanoparticles observed by TEM (Fig. 1). The broad peak at around 245 K should be due to the unblocking of the clusters of the magnetically coupled **2**–Fe_3O_4 nanoparticles. The magnetic dipole interaction between these coupled nanoparticles is indicated in the plot of $1/M$ as a function of temperature for the FC curve (Fig. 6e). Clearly, the data follow the Curie–Weiss law, $M \sim 1/(T-\theta)$. The sign and value of θ reflect the type and strength of the interaction. Here θ at approximately −300 K indicates a strong antiferromagnetic interaction. The broadness of the peak at 245 K should be due to the much broader size distribution of the clusters of the coupled nanoparticles.

The sharp increase in the magnetic moment at about 287 K again is due to the solid-to-hydrogel transition, at which the easy axes of the particles are aligned further by the magnetic field through physical rotation (which increases the magnetization) of the nanoparticles because the hydrogel is much softer and more elastic than the solid. Since the clusters (or the nanoparticles) not only interact with the

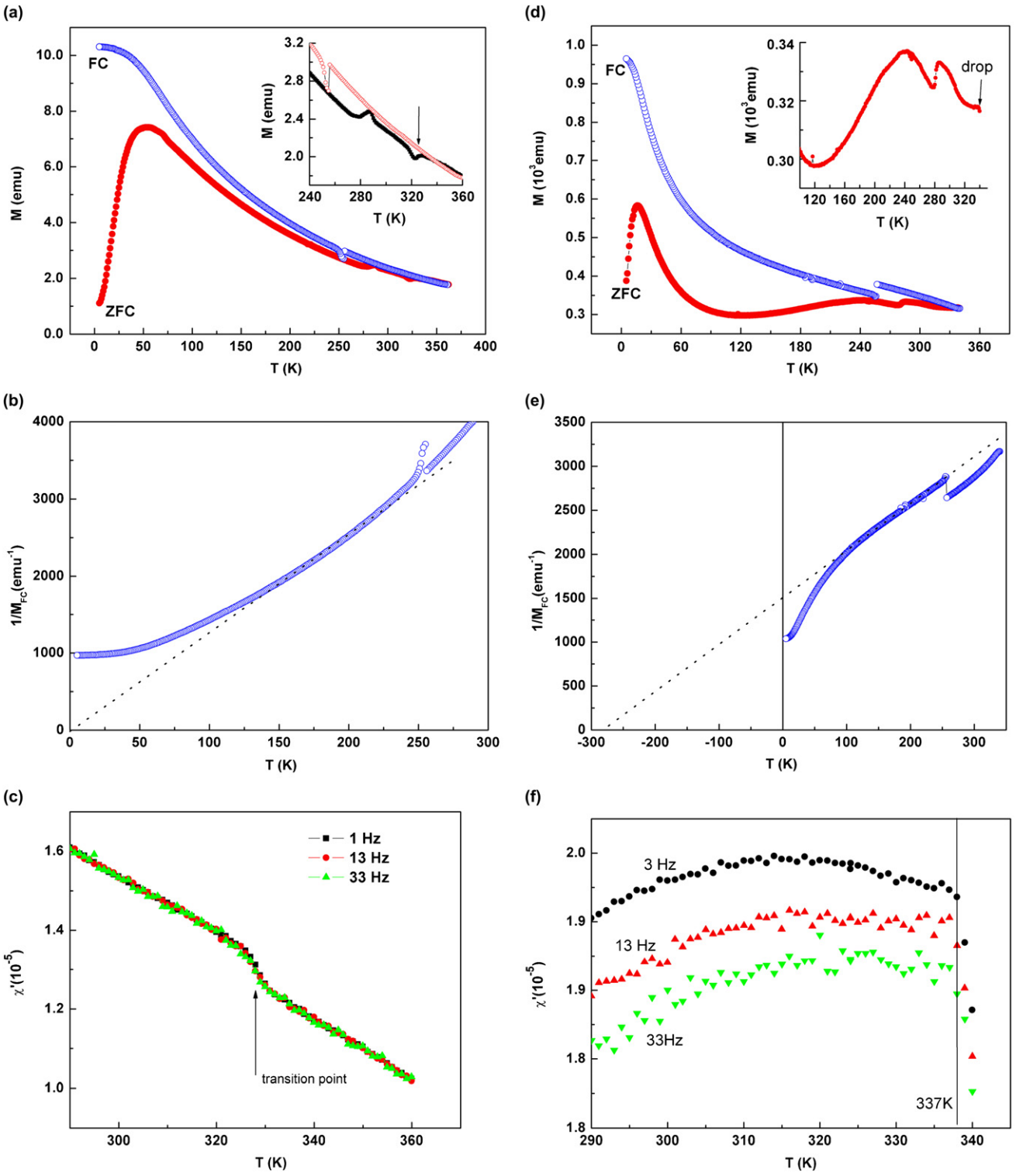

Figure 6. The magnetic characterization of the control (a, b, c) and the sample (d, e, f). (a, d) The ZFC–FC curves measured at 50 Oe; (b, e) the 1/*M* vesus *T* curves; (c, f) the magnetic susceptibility measured under an ac field with a field amplitude of 3 Oe.

hydrogelators in the nanofibers but also couple with each other magnetically due to the magnetic dipole interaction, the behavior of the nanoparticles above the blocking at 245 K does not follow the Curie law (Fig. 6e). The sharp drop in the magnetic moment at 337 K must be due to the gel–sol transition, which causes a dramatic frustration in the easy axes by releasing the magnetic torque or the Brownian motion of the nanofibers.

The ac susceptibility measurement also confirms the gel–sol transition. The mechanism of the susceptibility in the dc field and the ac field is quite different. In the dc field, the applied field attempts to align the magnetic moment of the particles in the field against thermal agitation and magnetic anisotropy, whereas when an ac field is applied, the magnetic moment follows the ac field and flip–flops. Therefore, a flip–flop of the moment can be achieved via the magnetic

moment flipping over the anisotropy barrier and/or via physical rotation. The ac susceptibility as a function of temperature measured with different frequencies is shown in Figure 6f. Peaks in the susceptibility curves appear at different temperatures for the different frequencies, which correspond to the unblocking of the clusters of the coupled particles as seen in the ZFC curve.[22] Above the peaks, the susceptibility decreases with increasing temperature and follows the Curie–Weiss law. The behavior of the susceptibility is clearly distinct from that of the control in the same temperature range (Fig. 6c). The sudden drop in susceptibility appears at 337 K, where the gel–sol transition occurs. The susceptibility indicates that the nanoparticles are restrained in the nanofibers, and their moments follow the change in the magnetic field only through over-barrier processes. The nanoparticles, however, move freely when the gel changes to a liquid (i.e., the Brownian motion can easily destroy the response of the moment to the ac field) and consequently the susceptibility drops dramatically.

Based on the magnetic characterization, we can infer the arrangement of the nanoparticles in the gel phase in the control and the sample. As illustrated in Scheme 4, the nanoparticles homogenously distribute outside the nanofibers of the hydrogelators in the control because of the lack of adequate supramolecular interactions between the DA–Fe_3O_4 nanoparticles and the nanofibers. On the contrary, the nanoparticles exclusively localize inside the hybrid nanofibers in the sample because of the sufficient supramolecular interactions between **2**–Fe_3O_4 nanoparticles and the hydrogelators. In other words, if we assume that the density of the hydrogelator is around 1 g/ml, the 0.8 wt % DA–Fe_3O_4 nanoparticles disperse in a greater than 98% volume fraction of the hydrogel in the control, but the 0.8 wt % **2**–Fe_3O_4 nanoparticles aggregate in a less than 2% volume fraction of the hydrogel in the sample. When the magnetic particles are coupled within the nanofibers, the magnetic interaction between the nanoparticles may serve as an extra stabilization force to maintain the hybrid nanofibers against Brownian motion. More importantly, upon the application of a small magnet, these coupled magnetic nanoparticles in the sample cooperatively move toward the magnet and break the hybrid nanofibers to exhibit the gel–sol transition. In the control, under a relatively small non-uniform magnetic field, the well-dispersed individual magnetic nanoparticles are unable to amass sufficient force to break the nanofibers of the hydrogelators and cause a gel–sol transition. The above results indicate that the arrangement/localization plays a more important role than the amount of the magnetic nanoparticles for generating magnetorheological hydrogels.

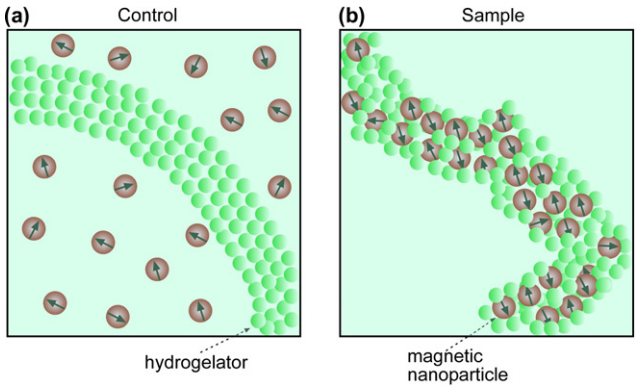

Scheme 4. The distribution and the localization of the magnetite nanoparticles in (a) the control and (b) the sample, respectively.

3. Conclusions

In conclusion, we have demonstrated a new type of magnetorheological material based on supramolecular interactions between low-molecular-weight hydrogelators and surface-modified magnetic nanoparticles. Compared to physically mixing nanoparticles into covalently cross-linked polymer hydrogels, our design has several distinct advantages: (i) the thermodynamically favored self-assembly process[23–29] permits the surface-modified magnetic nanoparticles to be integrated into the nanofibers; (ii) the supramolecular hydrogel requires only a small amount of the magnetic nanoparticles to exhibit a magnetoresponse; and (iii) a small magnetic force can modulate the self-assembled hybrid nanofibers and induce a phase transition. The mechanism revealed by the magnetic study in this work may also help in the design of other nanoparticle-based soft materials by using supramolecular interactions and self-assembly to generate localized/ordered domains/clusters of nanoparticles. Since hydrogels formed by molecular self-assembly are emerging as a new kind of biomaterial for drug delivery,[30–33] tissue engineering,[34–37] and biomineralization,[38,39] this magnetorheological supramolecular hydrogel, which consists of biocompatible magnetic nanoparticles, also signals the possibility of a new type of magnetoresponsive biomaterial.

4. Experimental

4.1. General

2-(Naphthalen-6-yl)acetic acid, DCC, DMAP, *N*-hydroxysuccinimide (NHS), L-phenylalanine, dopamine hydrochloride, benzyl bromine, Boc-anhydride, succinic anhydride, and trifluoro acetic acid (TFA) were purchased from Aldrich Co., and used without further purification. The TEM samples were prepared via cryo-drying for TEM on Philips CM20 and JEOL 2010. (The cryo-dried samples were prepared as follows: a copper grid coated with carbon was dipped into the hydrogel and placed into a vial, which was plunged into liquid nitrogen. Then, water was removed from the frozen specimen by a freeze-drier.) ^{1}H NMR spectra were obtained on 300 MHz Bruker. All the magnetic measurements were carried out on a Quantum Design SQUID magnetometer (MPMP-5s) equipped with a susceptometer and a 5 T magnet.

4.2. Synthesis

4.2.1. (*S*)-2-(2-(Naphthalen-6-yl)acetamido)-3-phenylpropanoic acid (1a). 2-(Naphthalen-6-yl)acetic acid (372 mg, 2 mmol) and NHS (230 mg, 2 mmol) were dissolved in 40 ml of chloroform, and DCC (453 mg, 2.2 mmol) and DMAP (13 mg, 0.1 mmol) were added to the above solution with stirring. After the reaction mixture was stirred at room temperature for 0.5 h, the resulting solid

was filtered off and the filtrate was evaporated in an open dish to dryness and the crude product was used in the next reaction without purification.

L-Phenylalanine (332 mg, 2 mmol) and $NaHCO_3$ (336 mg, 4 mmol) were dissolved in 20 ml of water with stirring, the solution of crude product (dissolved in 40 ml acetone/ethanol=1:1) was added, and the resulting reaction mixture was stirred at room temperature for 24 h. The reaction mixture was air-dried, then 30 ml of water was added and the precipitate was removed by filtration. The filtrate was acidified to pH~3 and the resulting product was obtained by filtration, washing with water, and then dried in vacuum. Compound **1a** (white powder) was collected with 84.2% yield (561 mg). ^{1}H NMR (300 MHz, DMSO-d_6): δ 7.84–8.01 (m, 3H), 7.75 (s, 1H), 7.60–7.67 (m, 2H), 7.22–7.36 (m, 6H), 4.87–4.91 (t, 1H), 3.64–3.72 (q, 2H), 2.76–3.02 (m, 2H). ^{13}C NMR (300 MHz, DMSO-d_6): δ 37.3, 42.7, 54.2, 126.0, 126.5, 126.9, 127.8, 127.9, 128.0, 128.1, 128.6, 129.7, 133.5, 134.5, 138.2, 170.4, 173.6. MS: calcd M^+=333.14, obsd $(M+1)^+$=334.21.

4.2.2. (*S*)-2-((*S*)-2-(2-(Naphthalen-6-yl)acetamido)-3-phenylpropanamido)-3-phenylpropanoic acid (1). Compound **1a** (333 mg, 1 mmol) and NHS (115 mg, 1 mmol) were dissolved in dimethoxy ethane (20 ml). After the solution was cooled to 0 °C in an ice-water bath, DCC (227 mg, 1.1 mmol) and DMAP (13 mg, 0.1 mmol) were added, and the reaction mixture was stirred for 4 h at 0 °C. After the resulting solid was filtered off, the filtrate was evaporated in an open dish to dryness and the crude product was used for the next reaction without purification.

L-Phenylalanine (166 mg, 1 mmol) and $NaHCO_3$ (168 mg, 2 mmol) were dissolved in water (10 ml) with stirring, the solution of crude product (dissolved in 20 ml of ethanol) was added, and the resulting reaction mixture was stirred at room temperature for 24 h. The reaction mixture was air-dried, then 20 ml of water was added and the precipitate was removed by filtration. The filtrate was acidified to pH~3.0, and the resulting solid product was isolated by filtration, washing by water, and then dried in vacuum. The product (white powder) was purified by flash chromatography (eluant: MeOH/$CHCl_3$=95:5), and 360 mg of product was obtained with the yield of 75%. ^{1}H NMR (300 MHz, DMSO-d_6): δ 7.89–8.05 (m, 3H), 7.79 (s, 1H), 7.62–7.68 (m, 2H), 7.18–7.40 (m, 11H), 4.91–4.95 (t, 1H), 4.64–4.67 (t, 1H), 3.66–3.74 (q, 2H), 2.74–3.07 (m, 4H). ^{13}C NMR (300 MHz, DMSO-d_6): δ 36.9, 38.1, 41.2, 53.6, 54.6, 125.7, 126.0, 126.8, 126.9, 127.3, 127.5, 127.9, 128.1, 128.3, 128.7, 129.0, 131.2, 133.7, 138.0, 171.6, 172.4, 173.6. MS: calcd M^+=480.20, obsd $(M+1)^+$=481.22.

4.2.3. *N*-[2-(3,4-Bis-benzyloxy-phenyl)-ethyl]-succinamic acid (2a). Compound **2a** was synthesized by the method described in Ref. 19.

4.2.4. *N*-[2-(3,4-Bis-benzyloxy-phenyl)-ethyl]-succinamic-L-phenylalanine (2b). Compound **2a** (433 mg, 1 mmol) and NHS (115 mg, 1 mmol) were dissolved in dimethoxy ethane (30 ml), and DCC (227 mg, 1.1 mmol) and DMAP (13 mg, 0.1 mmol) were added to the above solution with stirring. After the reaction mixture was stirred at room temperature for 24 h, the resulting solid was filtered off and the filtrate was evaporated in an open disk to dryness. The crude product was used for the next reaction without purification.

L-Phenylalanine (166 mg, 1 mmol) and $NaHCO_3$ (168 mg, 2 mmol) were dissolved in water (15 ml) with stirring, the solution of crude product (dissolved in 30 ml of ethanol) was added, and the resulting reaction mixture was stirred at room temperature for 24 h. The reaction mixture was air-dried, then 30 ml of water was added, and the precipitate was removed by filtration. The filtrate was acidified to pH~3.0, and the resulting product was isolated by filtration, washing with water, and then dried in vacuum. Product of 392 mg (white powder) was obtained with the yield of 67.5%. ^{1}H NMR (300 MHz, DMSO-d_6): δ 8.32 (d, 1H), 8.01 (t, 1H), 7.37–7.63 (m, 15H), 7.09–7.13 (t, 2H), 6.84–6.86 (d, 1H), 5.24–5.27 (d, 4H), 4.58 (q, 1H), 3.33–3.37 (t, 2H), 3.14–3.22 (dd, 1H), 2.96–3.04 (dd, 1H), 2.72–2.77 (t, 2H), 2.43–2.48 (t, 2H), 2.35–2.39 (t, 2H). MS: calcd M^+=580.26, obsd $(M+Na)^+$=603.26.

4.2.5. *N*-[2-(3,4-Bis-benzyloxy-phenyl)-ethyl]-succinamic-L-phenylalanyl-L-phenylalanine (2c). Compound **2b** (290 mg, 0.5 mmol) and NHS (58 mg, 0.5 mmol) were dissolved in dimethoxy ethane (15 ml). After the solution was cooled to 0 °C in an ice-water bath, DCC (115 mg, 0.55 mmol) and DMAP (7 mg, 0.05 mmol) were added, and the reaction mixture was stirred for 4 h at 0 °C. The resulting solid was removed by filtration, and the filtrate was evaporated in an open dish to dryness. The crude product was used for the next reaction without purification.

L-Phenylalanine (83 mg, 0.5 mmol) and $NaHCO_3$ (84 mg, 1 mmol) were dissolved in water (10 ml) with stirring, the solution of crude product (dissolved in 20 ml of ethanol) was added, and the resulting reaction mixture was stirred at room temperature for 24 h. The reaction mixture was air-dried and then water (20 ml) was added. After the precipitate was removed by filtration, the filtrate was acidified to pH~3.0 and the resulting product was isolated by filtration, washing with water, and then dried in vacuum. The product (white powder) was purified by flash chromatography (eluant: MeOH/$CHCl_3$=95:5), and 210 mg of product (white powder) was obtained with a yield of 58%. ^{1}H NMR (300 MHz, DMSO-d_6): δ 7.46–7.60 (m, 10H), 7.24–7.40 (m, 10H), 7.07–7.12 (t, 2H), 6.83–6.86 (d, 1H), 5.25 (d, 4H), 4.59–4.65 (m, 2H), 3.34–3.36 (t, 2H), 2.78–3.30 (m, 4H), 2.74 (t, 2H), 2.33–2.45 (m, 4H). MS: calcd M^+=727.33, obsd $(M+Na)^+$=750.32.

4.2.6. 3-[2-(3,4-Dihydroxy-phenyl)-ethylcarbamoyl]-L-phenylalanyl-L-phenylalanine (2). Compound **2c** (145 mg, 0.2 mmol) and Pd on active carbon (29 mg, 20 wt %) were placed in a 50 ml round bottom flask. After air was removed in vacuum, a mixture of chloroform and methanol (10 ml, 1:1) was added through a needle and a balloon with H_2 was placed over the reaction mixture. The reaction mixture was stirred at room temperature for 12 h. After the catalyst was filtered off through Celite, the product was obtained by removing the organic solvent and dried in vacuum. Product of 109 mg (pale yellow powder) was collected with a quantitative yield. ^{1}H NMR (300 MHz,

DMSO-d_6): δ 7.24–7.40 (m, 10H), 6.71–6.80 (m, 2H), 6.55–6.58 (d, 1H), 4.58–4.65 (m, 2H), 3.45–3.53 (m, 4H), 2.76–3.28 (m, 4H), 2.34–2.44 (m, 4H). ^{13}C NMR (300 MHz, DMSO-d_6): δ 31.0, 32.4, 36.2, 36.9, 37.6, 40.7, 53.6, 54.3, 114.8, 120.2, 126.5, 127.9, 128.2, 128.9, 133.6, 139.7, 143.7, 146.9, 172.0, 173.4, 175.6. MS: calcd M^+=547.23, obsd $(M+Na)^+$=570.22.

4.2.7. Fe_3O_4 nanoparticle–compound 2 conjugation (2–Fe_3O_4). Compound **2** (10 mg) was dissolved in 5 ml of mixture of chloroform and methanol, the solution of 5 ml hexane containing 10 mg magnetic nanoparticles was added to the above solution and the resulting mixture was sonicated for 5 h. The conjugate was obtained by centrifugation (12,000 rpm) and washed with methanol three times.

4.2.8. Fe_3O_4 nanoparticle–dopamine conjugation (DA–Fe_3O_4). Dopamine hydrochloride (10 mg) was dissolved in 5 ml of mixture of chloroform and methanol, the solution of 5 ml hexane containing 10 mg magnetic nanoparticles was added to the above solution and the resulting mixture was sonicated for 5 h. The conjugate was obtained by centrifugation (12,000 rpm) and washed with methanol three times.

References and notes

1. Klingenberg, D. J. *AIChE J.* **2001**, *47*, 246–249.
2. Ginder, J. M.; Davis, L. C. *Appl. Phys. Lett.* **1994**, *65*, 3410–3412.
3. Terech, P.; Weiss, R. G. *Chem. Rev.* **1997**, *97*, 3133–3159.
4. Estroff, L. A.; Hamilton, A. D. *Chem. Rev.* **2004**, *104*, 1201–1217.
5. Kiyonaka, S.; Sugiyasu, K.; Shinkai, S.; Hamachi, I. *J. Am. Chem. Soc.* **2002**, *124*, 10954–10955.
6. Zhang, Y.; Gu, H. W.; Yang, Z. M.; Xu, B. *J. Am. Chem. Soc.* **2003**, *125*, 13680–13681.
7. Yang, Z. M.; Gu, H. W.; Fu, D. G.; Gao, P.; Lam, K. J. K.; Xu, B. *Adv. Mater.* **2004**, *16*, 1440–1444.
8. Xing, B. G.; Yu, C. W.; Chow, K. H.; Ho, P. L.; Fu, D. G.; Xu, B. *J. Am. Chem. Soc.* **2002**, *124*, 14846–14847.
9. Hyeon, T. *Chem. Commun.* **2003**, 927–934.
10. Park, J.; An, K. J.; Hwang, Y. S.; Park, J. G.; Noh, H. J.; Kim, J. Y.; Park, J. H.; Hwang, N. M.; Hyeon, T. *Nat. Mater.* **2004**, *3*, 891–895.
11. Sun, S. H.; Murray, C. B.; Weller, D.; Folks, L.; Moser, A. *Science* **2000**, *287*, 1989–1992.
12. Sun, S.; Zheng, H. *J. Am. Chem. Soc.* **2002**, *124*, 8204–8205.
13. Zrinyi, M.; Barsi, L.; Szabo, D.; Kilian, H. G. *J. Chem. Phys.* **1997**, *106*, 5685–5692.
14. Xulu, P. M.; Filipcsei, G.; Zrinyi, M. *Macromolecules* **2000**, *33*, 1716–1719.
15. Szabo, D.; Szeghy, G.; Zrinyi, M. *Macromolecules* **1998**, *31*, 6541–6548.
16. Mayer, C. R.; Cabuil, V.; Lalot, T.; Thouvenot, R. *Angew. Chem., Int. Ed.* **1999**, *38*, 3672–3675.
17. Mayer, C. R.; Cabuil, V.; Lalot, T.; Thouvenot, R. *Adv. Mater.* **2000**, *12*, 417–420.
18. Yang, Z. M.; Liang, G. L.; Wang, L.; Xu, B. *J. Am. Chem. Soc.* **2006**, *128*, 3038–3043.
19. Xu, C. J.; Xu, K. M.; Gu, H. W.; Liu, H.; Zheng, R. K.; Zhang, X. X.; Guo, Z. H.; Xu, B. *J. Am. Chem. Soc.* **2004**, *126*, 9938–9939.
20. Zhang, X. X.; Hernandez, J. M.; Tejada, J.; Ziolo, R. F. *Phys. Rev. B* **1996**, *54*, 4101–4106.
21. Craik, D. *Magnetism: Principles and Application*; Wiley: Chichester, UK, New York, NY, 1995.
22. Zheng, R. K.; Gu, H. W.; Xu, B.; Zhang, X. X. *Phys. Rev. B* **2005**, *72*, 14416/1–14416/7.
23. Sun, Y. G.; Xia, Y. N. *Science* **2002**, *298*, 2176–2179.
24. Whitesides, G. M.; Grzybowski, B. *Science* **2002**, *295*, 2418–2421.
25. Kotov, N. A.; Dekany, I.; Fendler, J. H. *Adv. Mater.* **1996**, *8*, 637–640.
26. Glotzer, S. C.; Solomon, M. J.; Kotov, N. A. *AIChE J.* **2004**, *50*, 2978–2985.
27. Gates, B.; Xia, Y. *Appl. Phys. Lett.* **2001**, *78*, 3178–3180.
28. Redl, F. X.; Cho, K. S.; Murray, C. B.; O'Brien, S. *Nature* **2003**, *423*, 968–971.
29. Sun, S. H.; Anders, S.; Hamann, H. F.; Thiele, J. U.; Baglin, J. E. E.; Thomson, T.; Fullerton, E. E.; Murray, C. B.; Terris, B. D. *J. Am. Chem. Soc.* **2002**, *124*, 2884–2885.
30. Bhuniya, S.; Park, S. M.; Kim, B. H. *Org. Lett.* **2005**, *7*, 1741–1744.
31. Bhuniya, S.; Seo, Y. J.; Kim, B. H. *Tetrahedron Lett.* **2006**, *47*, 7153–7156.
32. Kiyonaka, S.; Zhou, S. L.; Hamachi, I. *Supramol. Chem.* **2003**, *15*, 521–528.
33. Yang, Z. M.; Liang, G. L.; Ma, M. L.; Abbah, A. S.; Lu, W. W.; Xu, B. *Chem. Commun.*, in press.
34. Yang, Z. M.; Xu, B. *Adv. Mater.* **2006**, *18*, 3043–3046.
35. Jayawarna, V.; Ali, M.; Jowitt, T. A.; Miller, A. E.; Saiani, A.; Gough, J. E.; Ulijn, R. V. *Adv. Mater.* **2006**, *18*, 611–615.
36. Yang, Z. M.; Ho, P. L.; Liang, G. L.; Chow, K. H.; Wang, Q. G.; Cao, Y.; Guo, Z. H.; Xu, B. *J. Am. Chem. Soc.*, in press.
37. Zhang, S. G.; Holmes, T. C.; Dipersio, C. M.; Hynes, R. O.; Su, X.; Rich, A. *Biomaterials* **1995**, *16*, 1385–1393.
38. Hartgerink, J. D.; Beniash, E.; Stupp, S. I. *Science* **2001**, *294*, 1684–1688.
39. Schnepp, Z. A. C.; Gonzalez-McQuire, R.; Mann, S. *Adv. Mater.* **2006**, *18*, 1869–1873.